

Metastable Intermediates in the Condensation of Semiflexible Polymers

B. Schnurr,^{1, 2, *} F. Gittes,^{1, 3, †} and F. C. MacKintosh^{1, 4, ‡}

¹*Department of Physics & Biophysics Research Division,
University of Michigan, Ann Arbor, MI 48109-1120*

²*Department of Physics of Complex Systems, Weizmann Institute of Science, Rehovot 76100, Israel*

³*Department of Physics, Washington State University, Pullman, WA 99164-2814*

⁴*Division of Physics and Astronomy, Vrije Universiteit, 1081 HV Amsterdam, The Netherlands*

Motivated by results from an earlier Brownian Dynamics (BD) simulation for the collapse of a single, stiff polymer in a poor solvent [B. Schnurr, F. C. MacKintosh, and D. R. M. Williams, *Europhys. Lett.* **51**(3), 279 (2000)] we calculate the conformational energies of the intermediate (racquet) states suggested by the simulations. In the absence of thermal fluctuations (at zero temperature) the annealed shapes of these intermediates are well-defined in certain limits, with their major structural elements given by a particular case of Euler's elastica. In appropriate units, a diagram emerges which displays the relative stability of all states, tori and racquets. We conclude that, in marked contrast to the collapse of flexible polymers, the condensation of semiflexible or stiff polymers generically proceeds via a cascade through metastable intermediates, the racquets, towards a ground state, the torus or ring, as seen in the dynamical simulations.

PACS numbers: 87.15.He, 36.20.Ey, 87.15.-v

I. INTRODUCTION

The conformation of individual polymer chains depends on the properties of their environment, *i.e.* the solvent [1, 2, 3]. In the presence of a *poor* solvent, isolated polymer chains tend to collapse toward compact states, in which polymer-solvent contacts are minimized. For flexible polymers, the kinetics of this coil-globule transition have been the subject of much research over the past few decades [4, 5, 6, 7, 8, 9]. The kinetic pathway for flexible polymer collapse has only recently been experimentally confirmed to involve the formation of a pearl necklace and the gradual diffusion of large pearls from the chain ends [10].

In contrast to the flexible case, many polymers exhibit substantial bending stiffness, thus adding the (opposing) tendency to form extended structures. This makes a compact globule energetically unfavorable for *semiflexible* polymers because compact globules involve large amounts of bending. Such chains are described by the persistent or worm-like chain (WLC) model [3], examples of which include predominantly biopolymers (*e.g.* F-actin and DNA) but also some synthetic polymers (*e.g.* kevlar). The balance between the tendencies to straighten the filament (due to a bending energy) and to condense it (due to an effective short-range attraction or poor solvent) is at the heart of the condensation of semiflexible polymers.

The apparent equilibrium collapsed state for semiflexible polymers is well-known: chains with significant bending stiffness can form rings or toroids to avoid incurring

the large bending penalty of a spherical shell or a globule. This condensed state has been suggested and studied theoretically [11, 12, 13, 14], demonstrated in a variety of experimental systems [15, 16, 17, 18, 19, 20], and confirmed by computer simulation [21, 22, 23, 24]. Theoretical work has predominantly addressed structural features such as the detailed packing of filaments [25, 26, 27, 28, 29, 30], while dynamical simulations and Atomic Force Microscopy (AFM) among others have increasingly focused on kinetic aspects and condensation intermediates [18, 19, 23, 31, 32].

A particular set of recent dynamical simulations of isolated chains [33] has strongly suggested a possible (and in fact generic) pathway for the collapse of semiflexible polymers. These simulations showed not only the eventual formation of tori from extended chains quenched in poor solvent but demonstrated a series of long-lived, partially collapsed intermediate states. Very similar chain morphologies (our racquet states) also appear in other simulation work [23] and AFM studies of DNA condensation [18]. Motivated by these results, we develop and analyze a hierarchical family of metastable racquet states. In particular, we demonstrate that their relative conformational energies are consistent with the role they play in the simulations: they form an energetically driven cascade of increasingly compact conformations with sharp transitions between them.

We begin in Section II with a brief summary of the dynamical simulation results [33] which motivated this analysis. Section III addresses the morphology and evolution of the shapes to be analyzed in the remainder of the paper. Our approach to calculating the surface contributions to the conformational energies is developed in Section IV, followed by the two main sections containing a detailed analysis of torus and racquet states (Sections V and VI respectively). Section VII finally compares their relative stability and discusses the qualitative agreement

*Electronic address: bernhard.schnurr@weizmann.ac.il

†Electronic address: gittes@wsu.edu

‡Electronic address: fcm@nat.vu.nl

with the dynamical simulation results we set out to understand.

II. BRIEF REVIEW OF THE DYNAMICAL SIMULATION RESULTS

The work described in Ref. [33] applied a standard Brownian Dynamics (BD) algorithm [2] to a bead-and-spring model of a single polymer chain in the plane to capture the most general features of a rather complex and biologically important process, the condensation of DNA. The technical details of that study are discussed elsewhere [33, 34]. Here, we merely sketch the gross features and the important generic results that motivated our work.

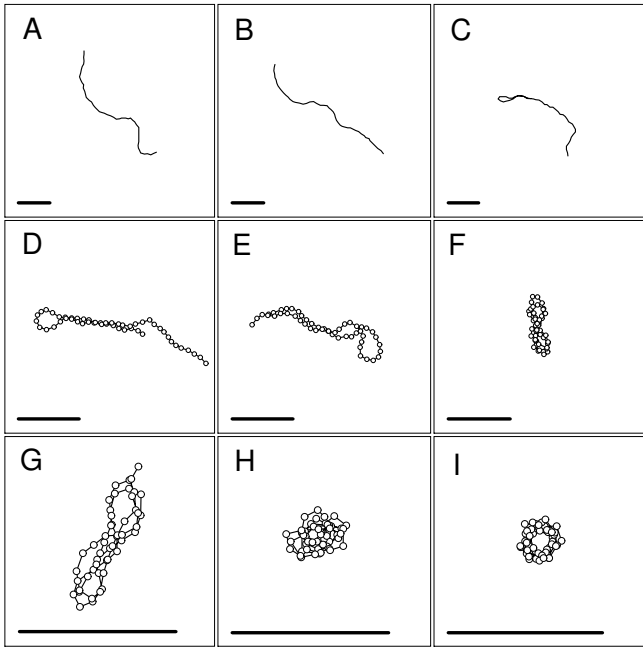


FIG. 1: Time evolution snapshots A–I of a single chain (50-mer, about $3 \ell_p$). The chain goes through various identifiable, temporally persistent stages: extended chain, single- and multiple-headed racquets, and finally the torus or ring. The scale bars are of one arbitrary length unit and indicate the increasing degree of magnification.

The dynamical evolution of a simulated chain followed a Langevin equation of the form

$$\xi \frac{dx_i}{dt} = -\frac{\partial U}{\partial x_i} + \eta_i(t) = F_{x_i} \quad (1)$$

for each bead i , where ξ is the coefficient of viscous drag ($\mathbf{F}_{\text{visc}} = \xi \mathbf{v}$) and η the random noise. Each bead is displaced by $\Delta x_i = (F_{x_i}/\xi)\Delta t$ during a time step Δt . The potential U contains all interactions internal to the chain, including the bending energy, a short-range attractive interaction between beads (mimicking poor solvent conditions) and a very stiff longitudinal compliance for each

bead-bead link along the chain. After thermalization of each chain, the solvent quality was quenched at $t = 0$.

Fig. 1 shows nine snapshots from a typical dynamical evolution of a relatively short chain of about three persistence lengths. The sequence shows a progression through well-defined stages identified by three types of conformations: extended chain (A–B), various racquet states (D–G), and finally the torus (I). For the same condensation event, Fig. 2 shows the end-to-end distance R_{e-e} of the filament as a function of time. Distinct changes in R_{e-e} coincide with conformational transitions: *e.g.* the rapid drop in the vicinity of C and D corresponds to the equalization of the two arms of a newly formed racquet. It is important to note that the described conformations persist in time, as seen by the quasi-plateaus in Fig. 2, each lasting for the considerable time of $\sim 10^6$ BD steps, about one tenth of the entire condensation event. We can roughly estimate the correspondence between our simulation steps and physical time for a particular system. To do this, we express the link length as a fraction of the persistence length and substitute for the local drag coefficient, assuming the viscosity of water. For F-actin, such an estimate suggests that an entire simulation of 10^7 BD steps models a filament for about 0.1 seconds. For DNA, this interval corresponds to a fraction of a millisecond.

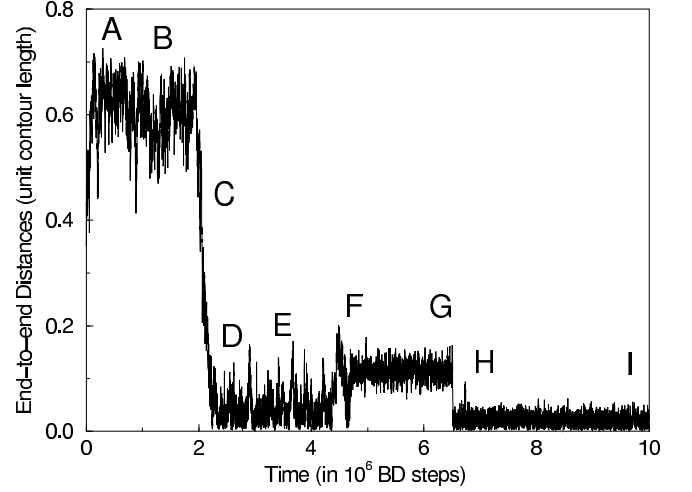


FIG. 2: End-to-end distances R_{e-e} versus time, for the same simulation sequence as in Fig. 1. The letters A through I roughly indicate the times at which the snapshots there were taken.

The temporal persistence of racquet structures is seen throughout the simulations, suggesting that metastable intermediates are a general feature in this collapse. Presumably, energy barriers between intermediates are responsible for their local (meta-)stability. We take it as evidence for the stability of the torus that no transitions were observed once the torus state was reached. This manuscript intends to shed some light on the energetics of the various stages in the condensation of a stiff polymer chain.

III. IDENTIFICATION OF INTERMEDIATE STATES

The dynamical simulations [33] suggest that the mechanism of collapse of semiflexible chains generically involves transitions through a series of long-lived intermediate states. In the absence of thermal fluctuations these intermediates anneal to certain underlying shapes which are well-defined and allow a straight-forward calculation of their conformational energies. For the single racquet, with a single loop at one end only, this annealed shape (Fig. 3) was produced in the simulation by slowly lowering the amplitude of the noise (or temperature) once the racquet had formed. This approach would also reveal the structure of the rod (the trivial case without any loops), all the racquet states, and the torus with various degrees of winding. Our calculations of the conformational energies and detailed shapes of these intermediates provide an insightful framework for understanding the simulation results.

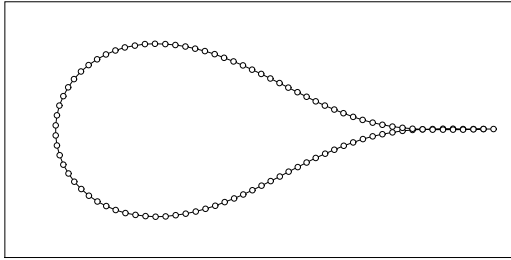


FIG. 3: Annealed shape of a racquet head from the BD simulation, achieved by slowly lowering the effective temperature once the structure has formed. The shape coincides with the analytical curve to within a line width.

In order to simplify the reference to specific states, we label all racquet states by their number of looped sections. Thus the rod is the $N = 0$ state, the racquet with a single loop at one end the $N = 1$, and so forth, as indicated in Fig. 4. We refer to the loop formed at the ends of the structure as the “head” and to the bundle of filaments connecting heads as the “neck”. For the moment we neglect the more subtle question of the exact location of filament ends. Naively one might assume that filament ends coincide with the ends of the neck, since it is straight; that is, the ends of the filament are expected to span the entire neck as they incur no bending penalty until they start bending into the head, but generally gain from increasing their overlap by reducing the solvent-exposed surfaces. We will see later on that this is not always so. However, the picture as described provides an adequate starting point for labeling the states we consider here. Among the shapes indicated in Fig. 4 we distinguish two basic racquet symmetries: those with even and odd numbers of heads N . For racquets with even N , the number of overlaps in the head sections is equal on the two sides, $p = q = N/2$. For racquets with odd N , one side (we arbitrarily call it the left, following

Fig. 4) has one less $p = (N - 1)/2$ overlap than the other (the right) with $q = (N + 1)/2$. As a consequence, the filament ends of an even racquet are on opposite sides of the neck, while those of an odd racquet are on the same side.

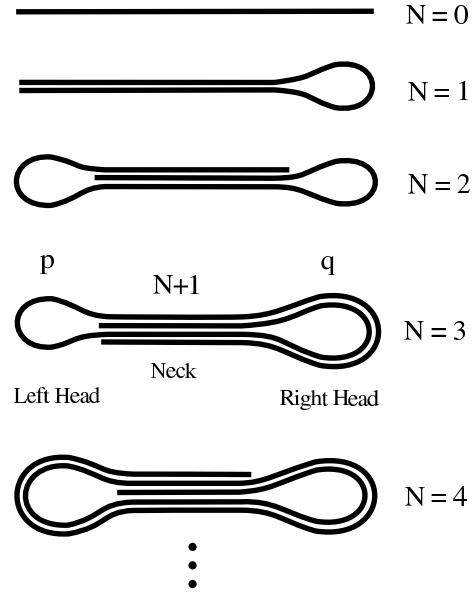


FIG. 4: Schematic “family” of racquet states for which we calculate conformational energies. The rod can be thought of as a trivial racquet without head ($N = 0$). All subsequent states are labeled by their numbers of head sections. Given enough filament, this series can be continued to arbitrary N .

Note that the dynamical simulations modeled the case of fixed experimental conditions. Neither filament length nor any other parameters were changed after the solvent quench. The polymer chain is merely exploring a given conformational energy landscape via thermal fluctuations. However, it can be instructive to consider as a *Gedankenexperiment* the case of variable filament length, especially in order to anticipate transition pathways between intermediates, and we use this perspective in our discussion. A (reduced) chain length is also a natural independent variable for the presentation and comparison of states. In this alternative perspective, the evolution of shapes starts with a short filament and gradually increase its length, effectively polymerizing the chain at one end. As the chain lengthens, only the neck follows at first until the formation of a new head is favored. The incremental unit of growth between conformations thus consists of one head plus one neck segment. This procedure can be continued to arbitrary N given enough filament. In Section IV C we will see that the appropriate formulation of the problem accomplishes changes in the (effective) filament length by adjusting the solvent quality instead of the actual chain length (a much more difficult experiment).

In the simulations, the actual transition into the torus

state could not be resolved in detail. It is clear however that there are in principle at least two ways in which a loop can form: two chain segments can meet with their tangent angles aligned at an angle of π or 2π . The former case leads to a racquet head, while the latter makes a ring that allows the chain to wind up into a torus directly. Since it is more likely for a stiff chain to bend into the smaller angle, one would expect the transition into racquets to be favored, at least for short chains. Statistically, the simulations [33] confirm this. Most of the chains studied there were relatively short (less than 10 persistence lengths) though a few examples (see Fig. 5) of longer chains showed qualitatively similar behavior, in addition to the intermittent display of superstructures of racquets within racquets.

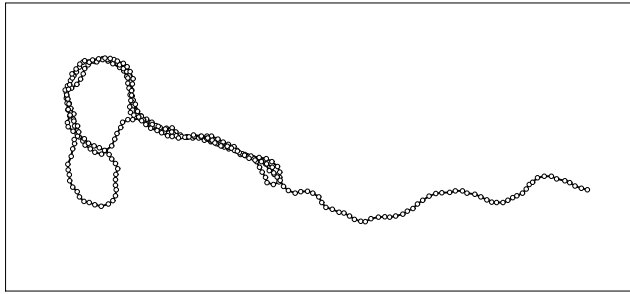


FIG. 5: Early stages in the evolution of a long chain (300-mer, roughly $20 \ell_p$) showing combinations of the conformational elements seen in shorter chains.

IV. CONFORMATIONAL ENERGIES

Having discussed the basic morphology of the intermediate states, we turn to the calculation of their conformational energies in the absence of thermal undulations. Racquet and torus conformations at zero temperature can be thought of as the underlying shapes, which become modified by fluctuations at finite temperatures. Apart from the bending contributions to the conformational energies, we need to describe the nature of the surface energy by which we model the poor solvent conditions that induce condensation. This surface energy assumes the packing or bundling of filaments in a hexagonal lattice (in cross section) and distinguishes between polymer and solvent exposure. The local arrangement into a hexagonal columnar phase has been confirmed for example by x-ray diffraction applied to bundles of DNA and other charged polymer chains [35, 36, 37, 38, 39] and the detailed structure within bundles of semiflexible polymer chains has been studied theoretically [40, 41].

Our calculations describe filaments of vanishing thickness compared to other length scales in the problem, while we model their packing on a hexagonal lattice. As implicit in the description of a worm-like chain, we assume a uniform bending modulus. In the torus state,

such an ideal chain forms a circular ring with a single radius of curvature. Furthermore, we assume for both racquet heads and torus that partial filament overhang, an effective non-uniformity in the bending modulus, does not change their shape but only their size. Neglecting these higher order corrections is certainly justified in the limit that the bundling number N gets large.

A. Surface Energy of Hexagonal Bundles

Although the Brownian Dynamics simulations [33] do not include this level of detail in the interaction between filaments, we treat filament bundles as hexagonally close-packed. Each filament in cross section can be thought of as having six sites occupied by either solvent or polymer. The poor solvent has the effect of lowering the energy for polymer-polymer relative to polymer-solvent contacts. To express the fact that there is a *relative* energetic advantage for filaments to bundle versus being exposed to solvent, we explicitly evaluate the total number of solvent-exposed sites and express the energy as a surface tension. Alternatively, one could use a reference state where the entire polymer chain is fully solvent-exposed and then subtract the effective shielding by bundle formation. Both approaches are valid and absolutely equivalent.

Particular surface energies are evaluated as follows. To find the coordination number α_N for an N bundle, consider the total number of surfaces or binding sites in the bundle with hexagonal order ($6N$). This number is proportional to the energy of N individual filaments completely exposed to solvent. To account for the effect of bundling, we note that a bond corresponds to the merging of two binding sites on neighboring filaments. We thus subtract the number of bonds formed from only half the number of sites ($3N$) to find the coordination number α_N . Multiplying by the surface tension parameter γ yields the surface energy per unit length for such a bundle. The numerology of this counting is summarized in Table I, listing bundling numbers, numbers of bonds per bundle, and their corresponding coordinations α_N up to $N = 31$.

B. Filled Shells and “Magic” Numbers

The list of coordination numbers in Table I bears the following general features. Differences between subsequent α_N are always either zero or one (except between $N = 1$ and 2). This creates differences (non-uniformities) in the effective binding strengths per unit length, thus favoring particular bundling numbers. We expect this effect for N with the same coordination as their predecessor ($\alpha_N = \alpha_{N-1}$) but a coordination of one less than the $(N+1)$ bundle ($\alpha_N + 1 = \alpha_{N+1}$). This is the case whenever an added filament adds three instead of two bonds, thereby filling a shell. Examples of this situation are

TABLE I: List of the bond numbers b_N and coordination numbers α_N in hexagonal packing for bundles of N up to 31. These numbers are referenced in the calculation of surface terms in the configurational energies for tori and racquets. “Magic” numbers representing particularly stable bundles are highlighted in boldface.

Bundling # N	Bond # b_N	Coordination α_N
1	0	3
2	1	5
3	3	6
4	5	7
5	7	8
6	9	9
7	12	9
8	14	10
9	16	11
10	19	11
11	21	12
12	24	12
13	26	13
14	29	13
15	31	14
16	34	14
17	36	15
18	39	15
19	42	15
20	44	16
21	47	16
22	49	17
23	52	17
24	55	17
25	57	18
26	60	18
27	63	18
28	65	19
29	68	19
30	71	19
31	73	20
:	:	:

found for $N = 7, 10, 12, 14, 16, 19, 21, 24, 27, 30\dots$ and we refer to them as “magic” numbers or filled shells. The reference to filled shells results from the geometrical observation that cross sections of magic numbers correspond to arrangements with high degrees of symmetry, as shown in Fig. 6.

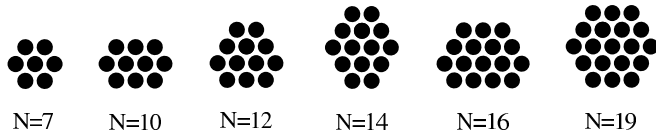


FIG. 6: Bundle cross sections of the lowest magic numbers (through $N = 19$) on a hexagonal lattice. Note the arrangements of the supermagic numbers 7 and 19 into perfect hexagons.

A few “supermagic” numbers ($N = 7, 19, 37\dots$) rep-

resent bundles with the special symmetry of the equilateral hexagon; we will not treat these cases separately. In agreement with Pereira and Williams [42] we find that bundles of magic numbers (and particularly the supermagic ones) play the role of preferred states with increased stability.

C. “Condensation” Length and Energy

The formulation of the problem as presented contains a characteristic length scale which greatly simplifies the discussion and presentation of our results. Balancing expressions for typical bending and surface energies ($\kappa/L \sim \gamma L$) for a given filament length L defines a measure we call the *condensation length* $L_c \equiv \sqrt{\kappa/\gamma}$. Its role in the behavior of a chain under particular conditions is the following: given the physical parameters κ and γ a filament much shorter than L_c will rarely self-intersect and therefore typically form an extended structure, while one much longer than L_c is likely dominated by overlaps and will form collapsed or at least partially collapsed (intermediate) structures.

Another combination of the two basic parameters κ and γ sets an analogous energy scale, the *condensation energy* $U_c \equiv \sqrt{\kappa\gamma}$. With these measures, all conformational energies U_N can be presented in dimensionless units, where physical energies and lengths are normalized by their condensation values. Expressing reduced conformational energies $u_N \equiv U_N/U_c$ as a function of reduced length $\lambda \equiv L/L_c$ renders the parameter space more manageable. This formulation also provides a convenient (experimental) realization of “changing the filament length”. Instead of changing the physical length of the chain, we vary λ by adjusting the values of κ and γ independently, presumably by changing the solvent quality while the intrinsic bending modulus remains constant.

V. TORUS STATES

We describe a torus by the following two (dimensionless) variables: a filament of length λ is wound into a circle of constant radius ρ , as shown in Fig. 7. In general, the torus can have any number N of complete windings (through an angle 2π) and an amount of extra overhang σ subject to the condition $\sigma < 2\pi\rho$. Since the entire filament contour length λ for this state has a constant curvature, the bending contribution to the conformational energy is always $\lambda/2\rho^2$.

We find it convenient to distinguish and label forms of the torus with different numbers of complete revolution N defined as the largest integer in $\lambda/2\pi\rho$. Any non-integer portion of this ratio represents overhang of filament beyond complete windings, defined as $\sigma \equiv \lambda - N(2\pi\rho)$. Our distinction of different tori by N naturally separates cases with different coordination numbers and

thus different surface energies. In anticipation of an important distinction that emerges, we call a torus without extra overhang ($\sigma = 0$) an “exact N ” while we refer to the generic torus with finite overhang ($\sigma \neq 0$) as an “ $N+$ ”.

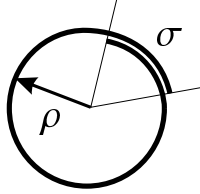


FIG. 7: Sketch of a generic torus (here a 1+ in our labeling scheme) of radius ρ and overhang σ to illustrate the description in the text. In general, the number of complete windings N can take on any integer value.

For the torus as described, we can then write down the following expression for its total conformational energy

$$u_N^{\text{torus}}(\lambda, \rho, \sigma) = \frac{\lambda}{2\rho^2} + 2\pi\rho [\alpha_N] + \sigma [\alpha_{N+1} - \alpha_N] \quad (2)$$

with the common bending term followed by two surface terms describing the contributions from the complete N -fold ring and the extra piece of overhang σ , respectively.

Substituting for σ leads to the torus energy in terms of λ and ρ only, which allows us to find the equilibrium size or radius $\rho_N(\lambda)$ for a particular state N by minimization with respect to ρ : note that $\partial^2 u_N^{\text{torus}} / \partial \rho^2 = 3\lambda/\rho^4$ is positive everywhere. Resubstitution of $\rho_N(\lambda)$ yields the conformational energy $u_N^{\text{torus}}(\lambda)$ in terms of the single variable λ . The expressions found in this way are valid in the ranges of λ between N and $N + 1$ times the circumference $2\pi\rho_N$. However, a real solution for this equilibrium size need not exist. This happens exactly for the magic numbers with $N \geq 12$. When a real solution for the equilibrium radius does exist, the resulting energy has two terms: one proportional to $\lambda^{1/3}$, the other to λ . The coefficient of the linear term is the combination of coordination numbers ($\alpha_{N+1} - \alpha_N$) which can vanish for N just below the magic numbers (at $N = 6, 9, 11, 13, \dots$) leaving these cases with the functional dependence $\lambda^{1/3}$ only. Another consequence of the numerology of hexagonal packing is that different states N can share the same energy expressions. Examples are the series $N = (2, 3, 4, 5)$ and the pairs $N = (7, 8), (17, 18), (22, 23), (25, 26), (28, 29), \dots$. These cases form a particular class of transitions where σ grows continuously with λ .

A. (Meta-)Stability

The above method for finding the optimal torus sizes by minimizing the conformational energy represents the conventional approach to determine metastability. However, there is a somewhat unusual aspect to the problem at hand. The energy expressions for torus states with

different N are in general not the same. This introduces discontinuities in the form of the energy between adjacent states. Consequently, there are not only the conventional minima identified by their vanishing slopes but also another class of solutions with discontinuities in slope at points where the energy expressions to the left and right differ due to the filament coordination. These are not minima in the usual sense (for instance, they are not locally quadratic minima); they are stabilized by finite slopes on both sides and do not have the usual signature of a vanishing slope. Our results for the tori are displayed in Fig. 8 and the limits of metastability for the various states are summarized separately in Table II.

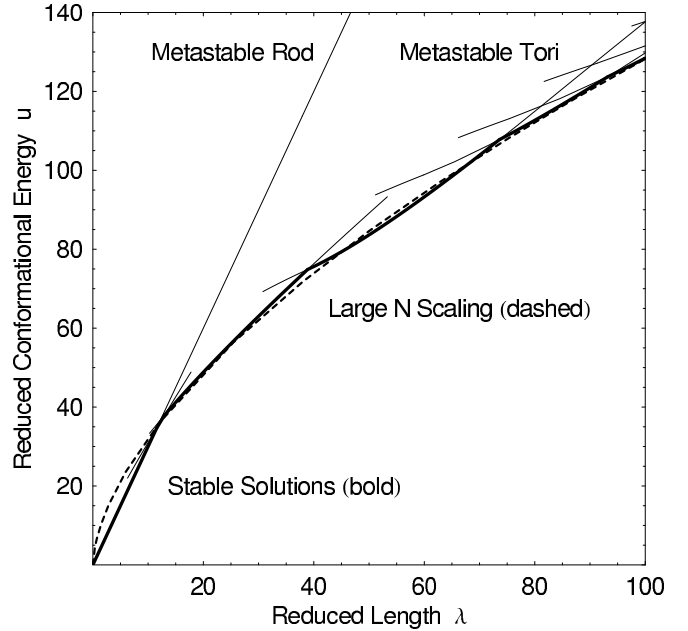


FIG. 8: Conformational energies of the torus states as a function of filament length in reduced units. Bold lines identify the ground states, while the dashed line shows the large N solution calculated in Section V D.

In order to establish the metastability of the tori of different N in more detail, we consider the behavior of the energy derivatives with respect to the radius $\partial u_N^{\text{torus}} / \partial \rho$ evaluated at the radii where the exact N and $N+1$ form. These derivatives are all monotonic functions (functional dependence: $-\lambda^{-2}$) with at most a single zero indicating a limit of metastability. Around these zeroes, the derivative is generically negative to the left and positive to the right. When negative (to the left), the energy is lowered by increasing the radius ρ , thus driving any overhang σ to vanish and making the torus an exact N . When positive (to the right) the opposite is true, driving σ to grow, making the torus an $N+$. Note that there are cases (notably again for the magic numbers with $N \geq 12$) where $\partial u_N / \partial \rho$ is negative everywhere. These cases form an important class in which tori never evolve (with increasing λ) towards states with finite overhangs: they remain metastable (with complete or exact overlap) for

TABLE II: Lower and upper limits of metastability (in terms of the reduced length λ) of the torus states for N up to 24. Series that are continuous in energy are separated by spaces, and states are labeled as N (exact) or $N+$. Note that tori with the magic numbers 12 and above are metastable to infinity (they grow as exact tori only).

N	Lower Limit	Upper Limit
0+	0	∞
1+	6.283	17.772
2+	10.260	18.850
3+	18.850	29.021
4+	29.021	40.558
5+	40.558	53.315
6+	30.781	38.789
7	38.789	82.283
7+	82.283	100.531
8+	100.531	119.958
9+	51.150	59.908
10	59.908	198.692
10+	198.692	229.229
11+	66.173	75.398
12	75.398	∞
13+	81.681	91.285
14	91.285	∞
15+	97.556	107.472
16	107.472	∞
17+	113.712	123.892
18+	123.892	134.358
19	134.358	∞
20+	140.496	151.164
21	151.164	∞
22+	157.250	168.092
23+	168.092	179.173
24	179.173	∞
:	:	:
:	:	:

all lengths beyond some lower limit. The relative positions of the zeroes in the energy derivatives combine in two fundamental ways, resulting in exact and $N+$ tori for various ranges of λ as summarized in Table II for the tori up to $N = 24$ (an arbitrary choice). A more complete discussion of the various cases can be found in [34].

The rod ($N = 0$) is of course a special (trivial) case without any bending contribution. Due to the absence of any competition between bending and self-affinity, the rod is (at least) metastable for all lengths and follows a straight line of slope 3λ (with the prefactor given by α_1). The next state is the $1+$. Its lower limit is given by the circumference of a single ring that just closes ($\lambda = 2\pi$), a circle with the radius of a condensation length. The subsequent small N states show variations of the basic elements depending on the numerology of the hexagonal coordination numbers. What emerges as the perhaps generic type of series for larger N is that of an $N+$ becoming an exact $N + 1$ which remains metastable to

infinity. All series we examined, starting with the $11+$ becoming an exact 12 , follow a similar pattern with slight variations due to neighboring tori sharing the same energy expression. It would appear that this remains the pattern for all larger N . Thus, in contrast to what we have emphasized here by treating only cases with relatively small N in detail, there appear to be only the few tori with N below 12 that show variations to the generic pattern of exact (magic N) tori without extra overhangs.

B. Stable Solutions or “Ground States”

The determination of the ground state is then straightforward, having established the energies of all the torus states and their limits of metastability. A direct comparison between relevant branches of the solutions provides the transition points between stable states and is summarized in Table III. These transitions are indicated in Fig. 8 by points between the bold line segments representing the ground states. The thinner lines indicate (metastable) solutions in regions where they are not the ground state.

TABLE III: Transition points for the lowest energy states (ground states) up to $N = 24$. Only for the “shortest” chains (λ up to 11.543) is the rod stable to the torus.

State Labels	Transition Points
0+ \longrightarrow 1+	11.543
1+ \longrightarrow 2+	12.957
2+ \longrightarrow 3+	18.850
3+ \longrightarrow 4+	29.021
4+ \longrightarrow 7	38.871
7 \longrightarrow 10	73.625
10 \longrightarrow 12	93.195
12 \longrightarrow 14	119.876
14 \longrightarrow 16	148.687
16 \longrightarrow 19	155.672
19 \longrightarrow 24	228.700
:	:

It appears that the majority of stable torus states (perhaps all $N \geq 12$, we have not checked systematically beyond $N = 24$) are exact states, meaning without overhang beyond the integral multiple of 2π over their entire range. Furthermore, their N are a subset of the magic numbers. In the range presented here, only the torus with $N = 21$ is skipped; all other magic numbers are ground states over some finite range of λ .

C. Discreteness

Another notable result are the discontinuities due to the hexagonal packing and its discrete coordination numbers. We might have expected the overhang σ and the torus size ρ to be continuous with changes in λ . At least

for small N we find instead that small changes in λ can cause discrete jumps in the size of the ring ρ . This characteristic has previously been described by Pereira and Williams [42]. To what extent these effects are experimentally observable is not known. As N grows large, the effect should weaken and ultimately disappear altogether.

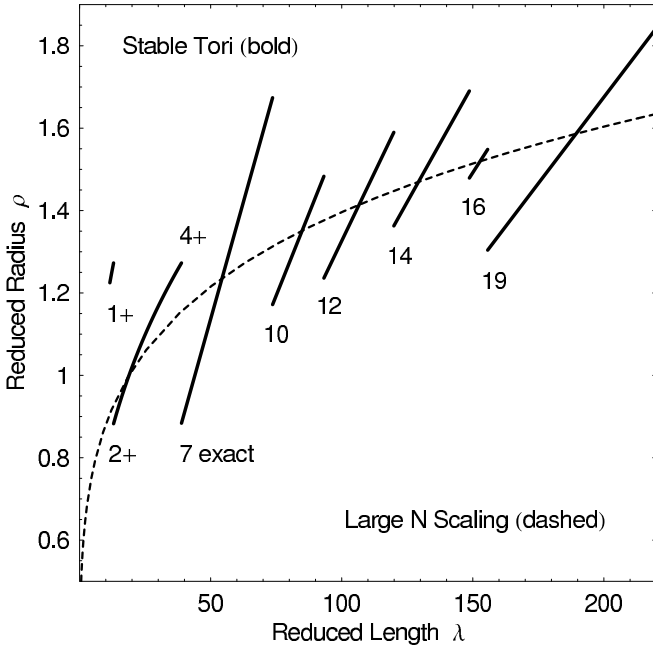


FIG. 9: Radii of the stable torus states (bold) as a function of filament length in reduced units, showing discrete transitions between the various series of states. The series shown are labeled by the states at their lower extremes. For comparison, the continuous large N solution is shown as a dashed line.

Discrete jumps are perhaps most prominently displayed as discontinuities in the torus size. Fig. 9 shows the sizes or radii $\rho_N(\lambda)$ of the ground states as a function of λ . The first bold curve segment starts where the filament first makes a stable $1+$ (at $\lambda = 11.543$) since ρ is not defined for the rod. Note that the functional dependence of the first two segments is different from the subsequent (linear) ones. The first two series evolve continuously according to their equilibrium solution for ρ_N with a functional dependence of $\lambda^{1/3}$. Their prefactors are determined by some combination of the appropriate coordination numbers. By contrast, all subsequent segments are due to solutions which are constrained to be exact (by virtue of the magic numbers) and thus have the linear dependence of $\lambda/2\pi N$. The length of the various segments indicates the stability of the states they represent. Clearly, states with supermagic bundling numbers (the figure only shows $N = 7$ and 19) are especially stable. The dashed line indicates the (continuous) solution found in the limit of large N , as discussed in the following section.

D. Large N Limit and Scaling

The scaling argument of the torus size with filament length goes back to Ubbink and Odijk [27]. We sketch a similar argument here in order to compare it in Section VID with the analogous argument for the racquets. First we give the straightforward scaling argument. In a second pass, we then determine the prefactors based on the more accurate, hexagonally faceted cross section of the torus.

In the limit as N grows large, we can neglect such details as partial overhangs (finite σ) since differences between N and $N + 1$ vanish as $1/N$. We assume first that the torus is a perfect cylinder with circular cross section. It grows as N , the number of filaments wound around its circumference. Thus, we expect the total torus surface area to scale as $\rho\sqrt{N}$. Substituting for the radius in a scaling sense ($\rho \sim \lambda/N$) we find that the conformational energy has two terms: one proportional to $\lambda/N^{1/2}$, the other to N^2/λ . Minimization with respect to N (implicitly letting N be a continuous variable) yields the following set of scaling relations.

$$N \sim \lambda^{4/5} \quad (3a)$$

$$\rho_\infty \sim \lambda^{1/5} \quad (3b)$$

$$u_\infty \sim \lambda^{3/5} \quad (3c)$$

To find the prefactors for these expressions, we need to consider a geometrically more careful treatment. We assume that the torus formed has both a perfect hexagonal cross section and an integer winding number (no partial overhangs). These assumptions are reasonable: it can be shown by direct calculation that the surface tension for a fixed number of filaments on a triangular lattice is smaller for the hexagonal than for the circular cross section. This is analogous to a Wulff construction [43] which captures, for instance, the faceting of crystals in solid state physics. The integer winding number is justified since the difference in the surface energies between N and $N + 1$ filaments vanishes as N becomes very large.

For an (equilaterally) hexagonal cross section with its symmetries, we can determine the following relationships geometrically. Given a hexagon made up of filaments at the vertices of a triangular lattice, we need to know both the number N of filaments contained in this structure as well as the number of solvent-exposed sites from the filaments at the surface, calculated as in Section IV A above. As a characteristic for the size of the hexagon, we label the integer number of lattice spacings on a side by m . The counting of lattice sites (or filaments) in such a hexagonal bundle is $N = 3m^2$ to leading order in m . The proper counting adds a linear and a constant term: $N = 3m^2 + 3m + 1$. In the limit of large N we keep only the leading order in m .

Using the same procedure as for the determination of coordination numbers, we find the surface energy of such a bundle by counting the number of solvent-exposed filament sites. A filament at an edge (of which there

are $m - 1$) exposes 2 sites, while one at a corner exposes 3. Taking into account the 6-fold symmetry of the hexagon, this results in $12m + 6$ exposed sites on the surface. Substituting the relation between m and N determined from hexagonal packing, we find the limiting coordination number (a surface energy per unit length) $\alpha_\infty = 2\sqrt{3}N$ for a hexagonal bundle of N close-packed filaments. This coordination number also provides the prefactors for the conformational energy of the torus in the limit of large N .

$$u_\infty = \frac{2\sqrt{3}\lambda}{\sqrt{N}} + \frac{2\pi^2 N^2}{\lambda} \quad (4)$$

The expressions analogous to Eqs. 3 with geometrical prefactors are

$$N = \frac{3^{1/5}}{(2\pi)^{4/5}} \lambda^{4/5} \approx 0.286 \lambda^{4/5} \quad (5a)$$

$$\rho_\infty = (6\pi)^{-1/5} \lambda^{1/5} \approx 0.556 \lambda^{1/5} \quad (5b)$$

$$u_\infty = \frac{5(3\pi)^{2/5}}{2^{3/5}} \lambda^{3/5} \approx 8.092 \lambda^{3/5}. \quad (5c)$$

The last two expressions are shown in Figs. 8 and 9 as dashed lines. We see outstanding agreement between the large N limit and the exact solutions down to the lowest N in Fig. 8.

VI. RACQUET STATES

The racquet conformational energies are made up of bending contributions from each of the heads, and surface contributions from the heads as well as the neck region in between. Any particular racquet state has well-defined coordination numbers throughout. As shown in Fig. 10, the racquets divide naturally into two groups: those with even and odd numbers N of total heads.

In the even case, the number of heads on each side equals $n \equiv N/2$ by symmetry. In the odd case, we have $p \equiv (N - 1)/2$ heads on the “left” and $q \equiv (N + 1)/2$ on the “right”. The labels “left” and “right” are our arbitrary naming convention (see Fig. 10) and are introduced to simplify the description of features such as the location of filament ends. The variables p and q for the bundling numbers of the heads always differ by 1 ($q = p + 1$) and sum to N . The bundling number of filaments forming the neck is always $N + 1$.

Given these bundling numbers, the remaining variables (in dimensionless units) for the generic racquet are the overall filament length λ , and the head sizes on the two sides (namely the contour lengths of the heads, labeled χ_p and χ_q). So far we have described the racquets with their filament ends coinciding with the ends of the neck. However, in general (and in analogy with the overhang σ in the torus case) we need to allow for the extension of these ends into the heads, or the retraction into the neck. Lengths of overhang are labeled σ_p and σ_q and their sign

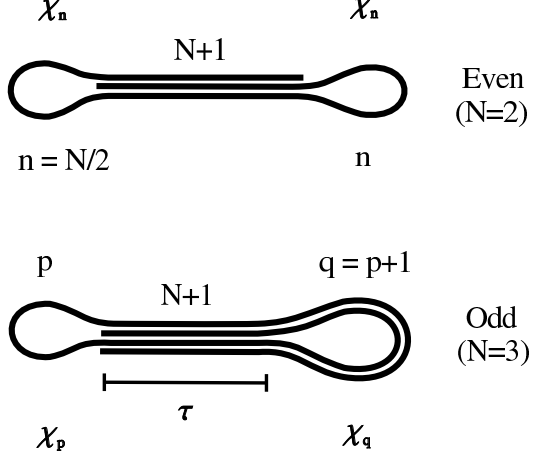


FIG. 10: Comparison of the structure and labels of generic even and odd racquets, represented here by the $N = 2$ and 3 . Note the symmetry between the heads in the even case, while the right side always has one additional head in the odd case. All the heads on a side are identical; the schematic separates head and neck filaments only to indicate their multiplicity.

indicates whether they extend into or retract back from the heads. The length of the neck τ is not an independent variable once all other parameters are fixed, since the total filament length imposes a constraint. Beyond this general description, we proceed by treating even and odd racquets separately, starting with the description of the more symmetrical even case.

For the even racquet with a given λ , the number of variables reduces to only two. Since the left and right heads for even racquets are identical by symmetry, we collapse their labels ($n \equiv p = q$) and are left with only one head size ($\chi_n \equiv \chi_p = \chi_q$) and a single overhang variable ($\sigma_n \equiv \sigma_p = \sigma_q$). The overall filament length for the even racquet is distributed into $\lambda_N^{\text{even}} = N\chi_n + 2\sigma_n + (N + 1)\tau$ where the terms are ordered as heads, overhang, and neck. For the odd racquet, we leave the left and right head sizes separate, but require that any overhang be symmetrically distributed on the left side. This is not the only possible metastable solution, but the one we describe here generically as the most symmetrical; we discuss the details of other possible solutions further in Section VI C. In the odd case, the overall chain length divides itself into $\lambda_N^{\text{odd}} = p\chi_p + q\chi_q + 2\sigma_p + (N + 1)\tau$ where we use the single overhang variable σ_p to indicate that the two possible pieces of overhang are always on the left side (see Fig. 10).

By way of a preview, we state here that the racquet solutions (see Fig. 11) differ fundamentally from those of the tori. While the size of the torus was found to increase as a function of λ (up to discontinuities), the sizes of the racquet heads (as well as any lengths of overlap) are fixed for each state by the local force balance between the bundles of filaments making up head and neck. Having determined the head sizes and overhangs for a particular

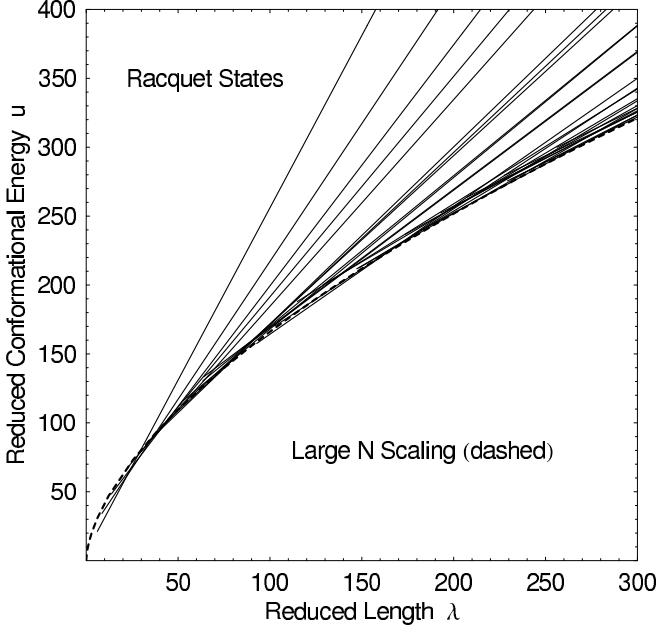


FIG. 11: Racquet state energies, shown as a function of filament length in dimensionless units, form a dense spectrum of solutions, each increasing linearly. The solid circles represent the lower limits of validity for each state. For comparison, the scaling solution with proper prefactor in the limit of large N is superimposed (dashed line). Note the nearly perfect agreement of the scaling solution with the lower envelope of the racquet states, down to the very lowest values of N .

state, its lower limit of validity λ_{low} is found by adding up the head sizes and overhangs in the absence of any neck at all ($\tau \rightarrow 0$). This is the minimal filament length required to form a particular racquet. For all lengths beyond, the racquets remain metastable as their energies increase linearly with slope $\alpha_{N+1}/(N+1)$ depending only on the bundling and coordination numbers in the neck. Adding extra filament to any racquet configuration only lengthens its neck, while the head sizes and any overhang remain fixed. As a consequence, all racquets are (at least) metastable solutions for any λ beyond their lower cutoff λ_{low} . What remains to formulate the total conformational energies of the racquets is the bending contribution due to partial overhangs.

A. Head Shape—an Elastica

Having identified the racquet head as the distinguishing common element among the intermediate states, we calculate its geometrical shape (see Fig. 12) in the absence of thermal fluctuations from the bending of a slender, elastic rod. Apart from the aesthetically pleasing nature of this solution, the formal expression for this head shape is necessary for the determination of bending energies for the racquets. The general class of shapes resulting from the bending of a slender rod by forces and cou-

ples applied at its ends only are known as *elastica*. Such solutions were first studied by Euler in 1744. The particular solution we seek is schematically drawn in Fig. 51 of the treatise by Love [44].

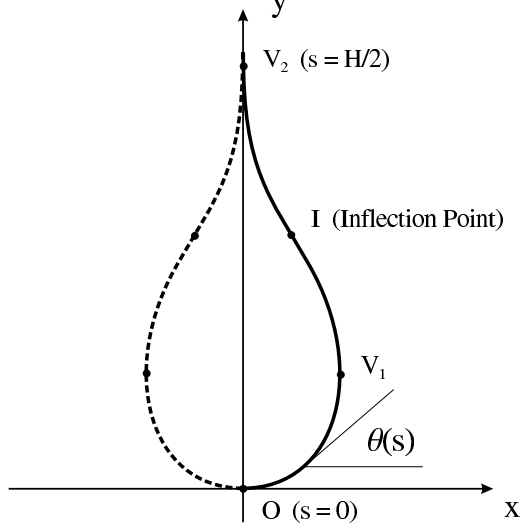


FIG. 12: Schematic figure of a racquet head with axes appropriate for our calculation. Local tangent angles θ are measured from the x axis. Symmetrical regions along the contour s are delimited by solid circles.

To solve for the shape of a racquet head of total contour length H we consider the geometry as shown and labeled in Fig. 12. In this section we use physical variables instead of the dimensionless units introduced previously, as they are more intuitive here and allow for dimensional analysis. Given the obvious symmetry about the y axis, it is sufficient to solve for one half of the racquet head only. The tangent angle along the curve is defined in such a way as to increase from $\theta = 0$ at the origin O ($s = 0$), via a maximum at the inflection point I , to $\theta = \pi/2$ at V_2 ($s = H/2$, where the head joins the neck). Note that there are two points V_1 and V_2 at which the tangent angle is vertical ($\theta = \pi/2$), with an inflection point I between them. These three points define an additional symmetry (about the inflection point I) for the contour between points V_1 and V_2 .

Our particular elastica is solved [45] by minimizing the WLC (worm-like chain) Hamiltonian subject to the boundary condition that the two halves of the head join in the neck at $x = 0$. We impose this constraint by means of a Lagrange multiplier ζ .

$$U = \int_0^{\frac{H}{2}} ds \left\{ \frac{\kappa}{2} \left(\frac{\partial \theta}{\partial s} \right)^2 + \zeta \cos \theta \right\} \quad (6)$$

Applying Euler's equation to this expression leads to the differential equation

$$\frac{d^2 \theta}{ds^2} = -\beta^2 \sin \theta(s) \quad (7)$$

where we made the substitution $\beta^2 \equiv \zeta/\kappa$ and expressed the angle $\theta(s)$ explicitly as a function of the contour length s . Note that the Lagrange multiplier ζ has the dimensions of a force and expresses the force required to join the two filament bundles in the neck balanced by the stiff filaments' intrinsic tendency to straighten out. Eq. 7 can be integrated to yield an expression for the curvature along the head contour s as a function of the tangent angle θ .

$$\frac{d\theta}{ds} = \frac{2\beta}{k} \sqrt{1 - k^2 \sin^2(\theta/2)} \quad (8)$$

Equivalently, one can rearrange terms and express the contour length s scaled by β in the form of an incomplete elliptic integral of the first kind $F(\phi, k)$

$$\beta s = k \int_0^{\frac{\theta}{2}} \frac{dt}{\sqrt{1 - k^2 \sin^2(t)}} = k F(\theta/2, k) \quad (9)$$

where k is the elliptic modulus (yet to be determined) and t an integration variable. This is the parametric solution of an elastica: it gives the contour length s as a function of the tangent angle θ . The expression is multivalued over its range, but invertible (one-to-one) in certain regions. Four such regions are defined by the axial symmetry of the head (through the origin and the neck) and the pair of inflection points in between. We thus cover the entire racquet head in a piecewise fashion, while only two of these regions are essentially different: the piece from O to V_1 and that from V_1 to I (with its reflection from I to V_2). The yet unknown elliptic modulus k for our elastica is found from a geometrical constraint. By the symmetry between the segments around the inflection point, we demand that the x value at point V_1 is twice that at the inflection point I . Solving the resulting equation numerically gives the value for the modulus as $k = 1.1695$. The inflection point is identified by the vanishing curvature of Eq. 8 (requiring $k \sin(\theta_I/2) = 1$) which corresponds to a tangent angle of $\theta_I = 2.052$.

The results so far give us complete if not very convenient information (in the form of elliptic integrals and parametric expressions) about the shape of our elastica. The expression for the curvature (in Eq. 8) allows us to evaluate the bending energy of such a racquet head. Since the bending energy (as evaluated in the WLC Hamiltonian) is an integral over the squared curvature, we can use Eq. 8 to evaluate this energy over any segment of the racquet head by integration. This requires the numerical evaluation of an incomplete elliptic integral of the second kind $E(\phi, k)$.

$$U = \frac{\beta\kappa}{k} \int d\theta \sqrt{1 - k^2 \sin^2(\theta/2)} = \frac{2\beta\kappa}{k} E(\theta/2, k) \quad (10)$$

Adding up the symmetrical pieces of this solution for the entire head yields the total bending energy of a complete racquet head $U^{\text{head}} = A(\kappa/H)$ with A representing the numerical constant 18.3331. Thus, the bending energy in a racquet head depends (apart from the value

for the bending modulus κ) only on its contour length. Note also that the bending energy of the racquet head is very close to (but slightly below) that of a circular ring with the same contour length H ($U^{\text{ring}} = 2\pi^2\kappa/H \approx 19.7392 \kappa/H$). Using circular rings as racquet heads would thus provide a reasonable approximation for the calculation of conformational energies, provided we neglect the penalty due to the sharp bends at the neck.

The form of the solution in Eq. 9 reveals that our racquet head shape or elastica is unique, in the sense that it is independent of any parameters in the problem. Both the parametric head shape $s(\theta)$ and the bending energy $U(\theta)$ are scaled by the factor β , related to the local force balance at V_2 . The overall size of the resulting shape is merely scaled up or down depending on the relative strength of the two competing tendencies, while its aspect ratio remains. Any slender, uniform rod, subject to these boundary conditions, will assume the described racquet head shape, whether it be microscopic or macroscopic. We emphasize that the size of the head is determined by a local condition, a balance of forces at the point where the filaments join to form the neck. Consequently the size of the racquet head does *not* depend on the overall filament length λ , as is the case for the torus, a major difference between the two types of conformational states. The dependence of the head size on the local force balance also suggests that the following experiment should be possible, at least in principle. Evaluating head sizes in a sample of partially condensed filaments would measure the local interaction strength between filaments, a quantity not easily found by other means. This approach assumes of course, that the value for the bending modulus (or equivalently the persistence length) is known from an independent measurement.

B. Bending Energy in Racquet Heads

To evaluate the bending contribution to the conformational energies we recall the expression for the bending energy in a head of size χ . Generalized to an N bundle (which effectively multiplies the bending modulus κ) the dimensionless bending energy for an N racquet head becomes $u_N^{\text{head}}(\chi) = A(N/\chi)$ where A is again the same numerical constant evaluated previously from elliptic integrals. A stability analysis and numerical minimizations found that "perfect" racquets (with $\sigma = 0$) are the solution for only a subset of all racquets.

In order to account for partial overhang into the heads (finite σ , as shown in Fig. 13), we need to generalize the notion of the numerical prefactor A . This "constant" is really a function of the partial overhang. Due to the scale invariance of our elastica, it is not surprising that A depends only on the *relative* overhang $\varsigma \equiv \sigma/\chi$. In terms of ς the four regions are delimited by the following values: 0, 0.1627, 0.5, 0.8373, and back to 1, measured from the neck. The three intermediate values identify the two inflection points and the halfway point (the ori-

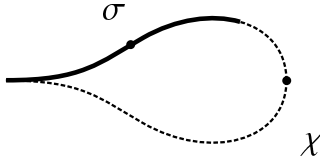


FIG. 13: Partial overhang σ (solid line) into an existing head of size χ (dashed). The ratio of σ/χ defines the fractional overhang ς . This schematic shows the typical situation for racquet solutions with nonzero overhang, with the filament end located somewhere between the inflection and the halfway points (solid circles).

gin in Fig. 12); note that these values are measured in the opposite sense from the one defined in the figure. Here, we follow the natural direction of increasing overhang. This requires some simple transformations when evaluating the elliptic integrals not in terms of angles but as functions of overhang lengths measured from the neck. In particular, we need to invert the original solution (Eq. 9) to find angles in each of the four regions separately (piecewise) and express them as functions of the partial overhang $\theta(\varsigma)$ with the proper directionality within each region. Reconstruction of the piecewise solutions for any amount of partial overhang σ yields the expression $u^{\text{partial}}(\sigma, \varsigma) = A(\varsigma)/\sigma$ with the numerical prefactor $A \equiv A(\varsigma = 1)$ generalized to the function $A(\varsigma)$.

C. Even and Odd Racquets

The surface energy terms for all racquets consist of several terms with different coordination numbers in general. The only term the even and odd cases share is the coordination in the neck, whose length τ is shared by $(N + 1)$ filaments. For the even racquet, symmetry simplifies the expressions somewhat. In each of its heads, we find a length $(\chi_n - \sigma_n)$ with coordination α_n and the overhang piece σ_n with coordination α_{n+1} while the neck has the common coordination α_{N+1} which leads to the full expression for the conformational energy of the even racquet.

$$u_N^{\text{even}} = A \left[\frac{N}{\chi_n} \right] + 2A(\sigma_n/\chi_n) \left[\frac{1}{\sigma_n} \right] + 2 [\alpha_n(\chi_n - \sigma_n) + \alpha_{n+1}(\sigma_n)] + \alpha_{N+1}(\tau) \quad (11)$$

The first two terms are the bending contributions for complete heads and partial overhang, while the three following terms are surface contributions for head segments and neck, respectively. For the odd racquets, the expression becomes

$$u_N^{\text{odd}} = A \left[\frac{p}{\chi_p} + \frac{q}{\chi_q} \right] + 2A(\sigma_p/\chi_p) \left[\frac{1}{\sigma_p} \right] + \alpha_p(\chi_p - 2\sigma_p) + \alpha_q(\chi_q + 2\sigma_q) + \alpha_{N+1}(\tau). \quad (12)$$

In the even case, there are only two free variables, χ_n and σ_n . We find their optimal values by simultaneous numerical minimization. In the odd case, the situation is slightly different, since we lack the symmetry between heads. However, we can make use of the fact that both filament ends (and therefore any potential overhang σ) are on the left side. This leaves the right head with a well-defined structure of q filaments in the head and $N + 1 = 2q$ filaments in the neck. Since the head size is solely determined by the respective bundling numbers in head and neck, we can determine right head sizes independently of any overhang on the left by minimization in terms of the various bundling and coordination numbers and A only.

$$\chi_q = \sqrt{\frac{2qA}{2\alpha_q - \alpha_{2q}}} \quad (13)$$

We then numerically minimize over the two remaining free variables χ_p and σ_p of the left head. Plotting constant energy contours as a function of the two free variables generally reveals the approximate location of the relevant minimum, and their coordinates were used as a starting point for the minimization routine. This procedure finds two possible outcomes for both the even and odd cases. In the simpler case, the energy is minimized without overhang ($\sigma = 0$) and we recover the naively assumed, perfect racquet structure. In the other case, we find a local minimum with respect to σ and χ for finite values of overhang, corresponding to metastable racquets with finite amounts of partial overhang σ . In every case we have checked (up to $N = 30$), these solutions put the fractional overhang in the second region of the racquet head, between the inflection and halfway points, as indicated in Fig. 13. Since we find only single minima for the N we examined, these minimizations solve the symmetrical, even cases.

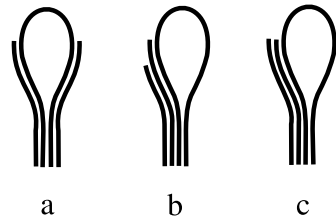


FIG. 14: Three possible solutions for partial overhang into the left head of an odd racquet. Case (a) is the one described in the text. The general case with different amounts of overhang on one side (b) is always minimized by the arrangement in case (c) where the two ends coincide.

Since both filament ends are on the same (left) side for the odd racquets, there are several possible configurations for overhang to be arranged, as shown in Fig. 14. The two pieces of equal length σ_p could be arranged symmetrically on opposite sides of the head. In another scenario, the two pieces of overhang are on the same side,

but not necessarily of equal length. All the cases we examined (up to $N = 30$) are minimized for one unique value of σ , corresponding to cases (a) and (c) in Fig. 14 which turn out to be degenerate in energy. In retrospect we were thus justified to describe the odd racquet with overhang generically as the symmetric case (a), while a second (asymmetrical) solution, degenerate in overhang and energy, exists.

All racquet head sizes χ_p and χ_q found either by direct calculation or by numerical minimization are displayed as a function of the racquet state label N in Fig. 15 to show the general trend and their convergence towards the large N solution. Head sizes typically increase with N , though not monotonically, and right heads are typically larger than left for the odd racquets. Even racquet heads are of course the same size, by construction.

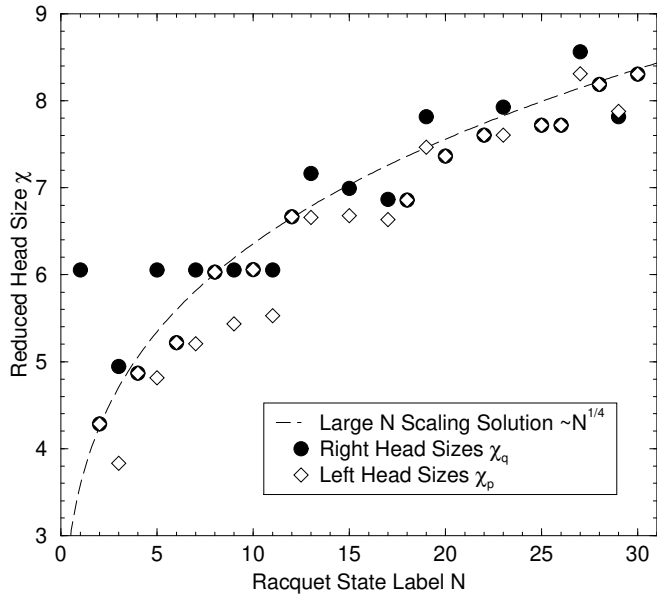


FIG. 15: Left and right head sizes versus the state label N . Pairs of even heads are of the same size, by symmetry. The general trend is for heads to grow with N , if not monotonically. Notice the convergence towards the asymptotic solution (dashed line, calculated in Eqs. 14) with increasing N .

Since our minimization allowed only for extension into the heads but not retraction of the filament ends back into the neck, we tested the stability of all racquets (up to $N = 30$) to these shape perturbations in the limit of small changes, subject to fixed overall length λ . We found three types of results. In the simplest case, the racquets are stable to any small change. These racquets (with $N = 1, 2, 3, 11, 15, 17, 20, 25, 28, 29\dots$) remain exact ($\sigma = 0$). A second class is identified by stability to retraction but not to extension. These racquets (with $N = 4 - 10, 13, 18, 22, 23, 26\dots$) develop finite (positive) overhang. The remaining cases are the magic numbers starting with 12 (namely $N = 12, 14, 16, 19, 21, 24, 27, 30\dots$) which are unstable (or marginal stable) to retraction along the neck. A subset of these states are unstable

to extension, and solutions with finite, positive overhang exist. However, those cases which are stable to extension have no metastable solution at all. We thus conclude that no racquet solutions exist for $N = 14, 16, 21, 24\dots$ and these states are omitted from our energy spectra (Fig. 11) and the series of head sizes (Fig. 15).

D. Large N Limit and Scaling

We perform the analogous calculation to that done for the torus states in Section VD, under the assumption that bundles form hexagonal cross sections as their bundling numbers N become large, to find the behavior of the racquet energies in the same limit. The result is shown as the dashed lines in Fig. 11 and Fig. 15. To compute it, we assume that the large N racquet be even and without overhang ($\sigma = 0$) as differences between bundles of nearly the same number of filaments vanish in this limit. This even racquet has a neck length τ and a limiting head size χ_∞ for large bundling numbers n in the heads and N in the neck (see Fig 16).

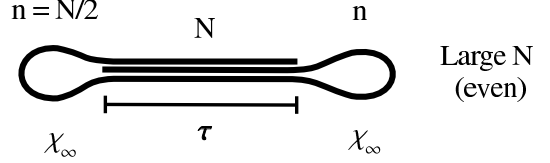


FIG. 16: Schematic racquet in the limit of large N where we assume the symmetry of the even racquet and neglect any extra overhang.

Since the size of the heads depends only on the local conditions (balance of forces) at the point where the head and neck bundles meet, we can calculate the optimal head size χ_∞ as in Eq. 13 for the right head of an odd racquet. As in Section VD, we determine the optimal bundling number $N_{\text{opt}}(\lambda)$ by minimizing the energy with respect to N , which yields the scaling results with prefactors as functions of λ only.

$$N_{\text{opt}} \approx 0.303 \lambda^{4/5} \quad (14a)$$

$$\chi_\infty \approx 2.653 \lambda^{1/5} \quad (14b)$$

$$u_\infty \approx 10.482 \lambda^{3/5} \quad (14c)$$

Knowing the head size χ_∞ from Eq. 14b, we can calculate the lower limit of validity λ_{low} in a scaling sense. This allows us to compare the expressions for the filament length from minimization ($\lambda_{\text{opt}} \approx 4.442 N^{5/4}$) with the length found by simply removing the neck altogether ($\lambda_{\text{low}} \approx 3.575 N^{5/4}$). Since the optimal length λ_{opt} exceeds the minimal length λ_{low} , a large N racquet will be one with a finite neck. This is an important result since it hints at the evolution of very long chains as they condense into racquets with increasingly larger N . In fact, we can estimate the growth of the neck length τ_∞

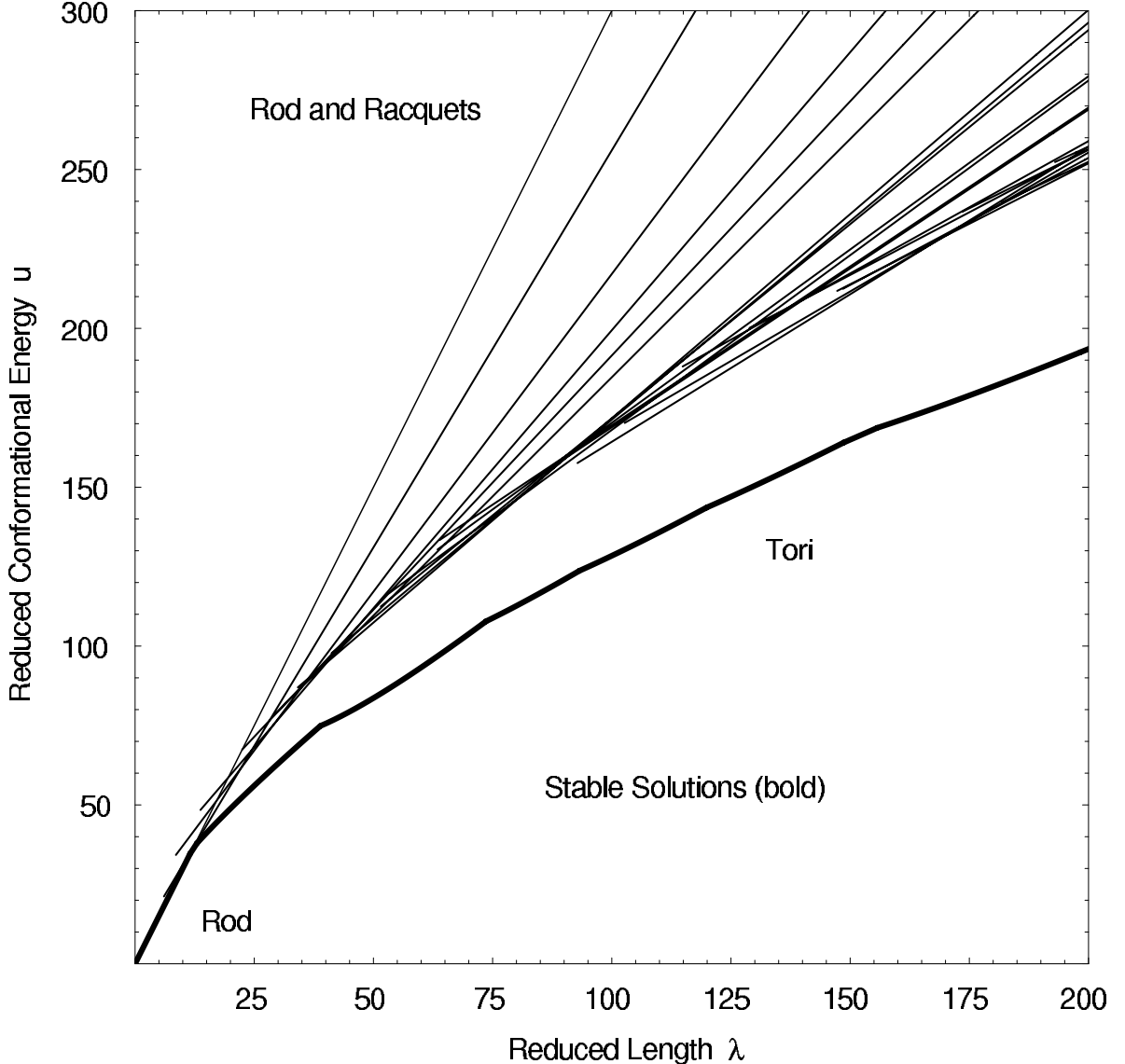


FIG. 17: Spectrum of rod, racquet and torus states shown as conformational energy versus filament length in reduced units. Only the rod (at small λ) and the tori (for all λ beyond a transition point) are globally stable states. Notice the rather large gap between the spectrum of racquet states and the stable torus solution. Metastable torus solutions are omitted for clarity.

from the difference between the prefactors in λ_{low} and λ_{opt} . Its scaling is given by $\tau_\infty \approx 0.644 \lambda^{1/5}$. Thus, the neck grows with the same power of λ as the heads but with a smaller prefactor. We may have anticipated that the growing heads provide a simple pathway towards the torus, as the inevitable limit of the heads growing at the expense of the neck. For a fixed filament length, the neck would have had to shrink to zero with increasing N , opening the structure up to form a torus. However, since the neck grows with the same power of λ , this pathway is not as compelling. For the particular racquet solutions shown in Fig. 11 we notice that the end points are relatively dense and represent, at times, the lowest point in the spectrum of states. Especially for such states, it is still true that their neck can shrink to very small or

vanishing lengths, depending on λ . Thermal fluctuations can then lead to the opening up of the neck to form a torus. Yet, even if the limit of large N does not provide an absolutely compelling pathway for the collapse to the torus, we now appreciate the energetics involved.

VII. DISCUSSION: RACQUETS VERSUS TORI

Fig. 17 shows the individual racquet solutions of Fig. 11 now compared to the stable torus ground states found in Section V B. In anticipation of those results, we described the lowest metastable torus state over any range of λ as the ground state of the system. Fig. 17 confirms this claim by direct comparison of racquets and

tori. In addition, we found that the large N solutions for tori and racquets both grow as $\lambda^{3/5}$ but with different prefactors. In combination with the close agreement between particular solutions and the large N limit, this strongly suggests that the torus remains the ground state for all λ beyond the transition point ($\lambda = 11.543$). Only for shorter chains is the rod the ground state.

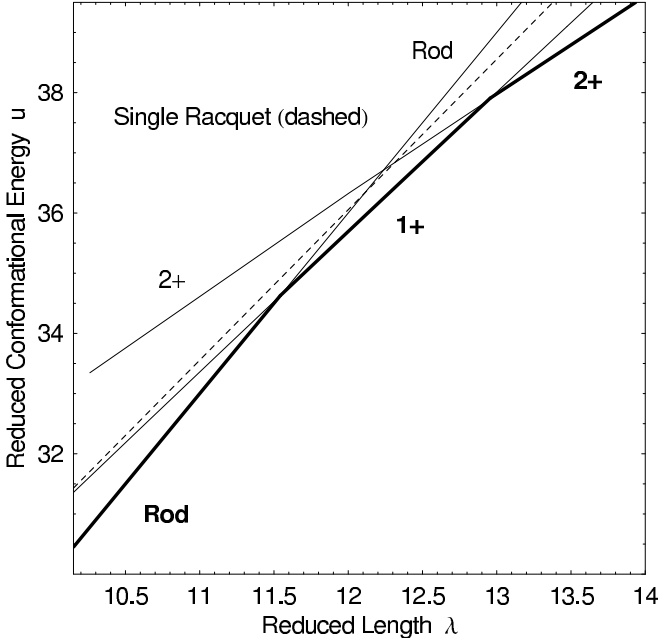


FIG. 18: Close-up of the rod, racquet and torus solutions in the region where they are closest to each other. Racquets are indeed never stable, though their energy is very close to both the rod and the torus in this region. Stable (ground state) solutions thus exist for rod and torus only.

There appears to be only one region where the energies of racquets and tori are even close, at the very low values of λ near the transition point. Fig. 18 shows the relevant region in detail. The $N = 1$ racquet solution comes extremely close to the solutions for both the rod ($N = 0$) as well as the $1+$ torus, but remains above. Thus the only stable (ground state) solutions for this system (in the absence of thermal fluctuations) are the rod at small λ and the tori everywhere beyond the transition point. At energies above this ground state, we see a dense spectrum of metastable solutions, made up of other (metastable) torus (see Fig. 8 for details) and increasing numbers of racquet states.

For fixed conditions (constant λ) we need only consider a vertical slice through the spectrum of energies. Along such a line, we can imagine a filament cascading down from an extended, rod-like configuration, through vari-

ous metastable intermediates, while lowering its energy along the way. Our calculations do of course not capture the entire physical picture, as our states are calculated in the absence of thermal undulations. We have so far not estimated the energy barriers between the metastable intermediates. However, based on the dynamical simulation results [33] it does appear that filaments at finite temperature do naturally cascade down through the spectrum of states. Some of the chains get “stuck” in various metastable racquet states, while others reach the torus ground state even within the relatively short simulation time. The large energy difference between the spectrum of racquets and the torus ground states is at least partially responsible for this strong tendency. This gap also stabilizes the ground state considerably. The results of our analysis thus nicely corroborate at least qualitatively the results of the computer simulation and its features relevant to the condensation of stiff chains.

We would like to note that the shape of condensed filaments may depend on the nature and molecular structure of the condensing agent. Our study only addresses an interaction that is uniform along the filament, such as the effect due to a poor solvent. Other systems, with more point-like organizing centers, have been shown to exhibit intricate multi-leaf or flower patterns [31, 46].

Our observations suggest that the pathway for the collapse of extended chains into condensed structures via intermediate racquet states is a viable, even generic alternative to the perhaps more immediately guessed direct winding up upon the meeting of filament ends at an obtuse angle. Some of the simulations show this latter collapse pathway, but it is much less frequent. Furthermore, this cascade picture through which our calculations reinforce and at least partially explain the simulation results, seems robust. We find this cascade through intermediate states even for a much more naive treatment of the poor solvent interaction used in a first pass. The individual curves (e.g. in Fig. 17) are shifted but show a qualitatively similar picture. The generic cascade through metastable intermediates is so dominant to be retained regardless of the detailed realization of the interactions.

Acknowledgments

The authors wish to thank David Williams for helpful discussions, including sharing aspects of related work [42]. This work was supported in part by the Whitaker Foundation and by NSF Grant Nos. DMR-9257544, INT-9605179. BS acknowledges support from the Minerva Foundation (Max Planck Society).

[1] P.-G. deGennes, *Scaling Concepts in Polymer Physics* (Cornell University Press, Ithaca, 1979).

[2] M. Doi and S. F. Edwards, *The Theory of Polymer Dynamics* (Clarendon Press, Oxford, 1988).

- [3] A. Y. Grosberg and A. R. Khokhlov, *Statistical Physics of Macromolecules*, AIP Series in Polymers and Complex Materials (AIP Press, New York, 1994).
- [4] P. G. deGennes, *J Phys Lett - Paris* **46**, L639 (1985).
- [5] B. Ostrovsky and Y. Bar-Yam, *Europhys. Lett.* **25**, 409 (1994).
- [6] A. Buguin, F. Brochard-Wyart, and P. G. deGennes, *Comptes Rendus de l'Académie des Sciences Série II Fascicule B - Mécanique Physique Chimie Astronomie* **322**, 741 (1996).
- [7] K. A. Dawson, E. G. Timoshenko, and Y. A. Kuznetsov, *Physica A* **236**, 58 (1997).
- [8] A. Halperin and P. M. Goldbart, *Phys. Rev. E* **61**, 565 (2000).
- [9] N. Lee and D. Thirumalai, *Macromolecules* **34**, 3446 (2001).
- [10] B. Chu, Q. C. Ying, and A. Y. Grosberg, *Macromolecules* **28**, 180 (1995).
- [11] A. Y. Grosberg, *Biofizika* **24**, 32 (1979).
- [12] V. A. Bloomfield, *Biopolymers* **31**, 1471 (1991).
- [13] V. A. Bloomfield, *Biopolymers* **44**, 269 (1997).
- [14] V. V. Vasilevskaya, A. R. Khokhlov, S. Kidoaki, and K. Yoshikawa, *Biopolymers* **41**, 51 (1997).
- [15] A. Z. Li, T. Y. Fan, and M. Ding, *Sci. China Ser. B-Chem.* **35**, 169 (1992).
- [16] Y. Fang and J. H. Hoh, *Nucleic Acids Res.* **26**, 588 (1998).
- [17] M. R. Shen, K. H. Downing, R. Balhorn, and N. V. Hud, *J. Am. Chem. Soc.* **122**, 4833 (2000).
- [18] A. L. Martin, M. C. Davies, B. J. Rackstraw, C. J. Roberts, S. Stolnik, S. J. B. Tendler, and P. M. Williams, *FEBS Lett.* **480**, 106 (2000).
- [19] D. Liu, C. Wang, Z. Lin, J. W. Li, B. Xu, Z. Q. Wei, Z. G. Wang, and C. L. Bai, *Surf. Interface Anal.* **32**, 15 (2001).
- [20] H. G. Hansma, *Annu. Rev. Phys. Chem.* **52**, 71 (2001).
- [21] H. Noguchi, S. Saito, S. Kidoaki, and K. Yoshikawa, *Chem. Phys. Lett.* **261**, 527 (1996).
- [22] A. Byrne, E. G. Timoshenko, and K. A. Dawson, *Nuovo Cimento della Societa Italiana di Fisica D* **20**, 2289 (1998).
- [23] H. Noguchi and K. Yoshikawa, *J. Chem. Phys.* **113**, 854 (2000).
- [24] M. J. Stevens, *Biophys. J.* **80**, 130 (2001).
- [25] N. V. Hud, *Biophys. J.* **69**, 1355 (1995).
- [26] N. V. Hud, K. H. Downing, and R. Balhorn, *Proc. Natl. Acad. Sci. U. S. A.* **92**, 3581 (1995).
- [27] J. Ubbink and T. Odijk, *Biophys. J.* **68**, 54 (1995).
- [28] J. Ubbink and T. Odijk, *Europhys. Lett.* **33**, 353 (1996).
- [29] S. Y. Park, D. Harries, and W. M. Gelbart, *Biophys. J.* **75**, 714 (1998).
- [30] V. L. Golo, E. I. Kats, and Y. M. Yevdokimov, *Journal of Biomolecular Structure & Dynamics* **15**, 757 (1998).
- [31] Y. Fang and J. H. Hoh, *J. Am. Chem. Soc.* **120**, 8903 (1998).
- [32] S. Q. He, P. G. Arscott, and V. A. Bloomfield, *Biopolymers* **53**, 329 (2000).
- [33] B. Schnurr, F. C. MacKintosh, and D. R. M. Williams, *Europhys. Lett.* **51**, 279 (2000).
- [34] B. Schnurr, Ph.D. thesis, University of Michigan (2000).
- [35] Y. M. Yevdokimov, A. L. Platonov, Y. M. Varshavsky, and A. S. Tikhonenko, *FEBS Lett.* **23**, 180 (1972).
- [36] T. Maniatis, J. H. Venable, and L. S. Lerman, *J. Mol. Biol.* **84**, 37 (1974).
- [37] Y. M. Yevdokimov, T. L. Pyatigorskaya, O. F. Polyvtsev, N. M. Akimenko, V. A. Kadykov, D. Y. Tsvankin, and Y. M. Varshavsky, *Nucleic Acids Res.* **3**, 2353 (1976).
- [38] R. Podgornik, D. C. Rau, and V. A. Parsegian, *Macromolecules* **22**, 1780 (1989).
- [39] R. Podgornik and V. A. Parsegian, *Macromolecules* **23**, 2265 (1990).
- [40] T. Odijk, *Biophys. Chem.* **46**, 69 (1993).
- [41] T. Odijk, *Europhys. Lett.* **24**, 177 (1993).
- [42] G. G. Pereira and D. R. M. Williams, *Europhys. Lett.* **50**, 559 (2000).
- [43] G. Wulff, *Zeitschrift für Kristallographie* **34**, 449 (1901).
- [44] A. E. H. Love, *A Treatise on the Mathematical Theory of Elasticity* (Dover Publications, New York, 1944).
- [45] F. Gittes, Ph.D. thesis, University of Washington (1994).
- [46] H. Schiessel, J. Rudnick, R. Bruinsma, and W. M. Gelbart, *Europhys. Lett.* **51**, 237 (2000).